Nanograin effects on the thermoelectric properties of poly-Si nanowires

N.Neophytou[1], X.Zianni[2,3], M. Ferri[4], A. Roncaglia[4], G.F. Cerofolini[5], and D. Narducci[5,6]

[1]Institute for Microelectronics, Technical University of Vienna, Austria.

[2]Dept. of Applied Sciences, Technological Educational Institution of Chalkida, 34 400 Psachna, Greece.

[3]Institute of Microelectronics, NCSR 'Demokritos', 153 10 Athens, Greece.

[4]IMM-CNR, Bologna, Italy.

[5]Dept. of Materials Science, Univ.of Milano–Bicocca, via R. Cozzi 53, 20125 Milano, Italy.

[6]Consorzio DeltaTi Research, Milano, Italy.

ABSTRACT

In this work we perform a theoretical analysis of the thermoelectric performance of polycrystalline Si NWs by considering both electron and phonon transport. The simulations are calibrated with experimental data from monocrystalline and polycrystalline structures. We show that heavily doped polycrystalline NW structures of grain size below 100nm might offer an alternative approach to achieve simultaneous thermal conductivity reduction and power factor improvements through improvements in the Seebeck coefficient. We find that deviations from the homogeneity of the channel, and/or reduction in the diameter may provide strong reduction in the thermal conductivity. Interestingly, our calculations show that the Seebeck coefficient and consequently the power factor can be improved significantly once the polycrystalline geometry is properly optimized, while avoiding strong reduction in the electrical conductivity. In such a way, *ZT* values even higher than the ones reported for monocrystalline Si NWs can be achieved.

I. INTRODUCTION

Silicon nanowires (NWs) have attracted significant attention as efficient thermoelectric materials mostly due to significant reduction in their thermal conductivity. Recent experimental measurements reported thermal conductivity values as low as κ_l=1-2W/mK in Si NWs with diameters below 50nm, which resulted in an impressive ZT~1, compared to Si bulk ZT_{bulk}~0.01 [1, 2]. As of now, however, no benefits were observed through the power factor. Moreover, experimental efforts were not able to achieve a significant relaxation of the adverse interdependence between the electrical conductivity and the Seebeck coefficient. In order to achieve higher performance, however, efforts need to be directed towards power factor improvements as well, since the thermal conductivity in nanostructures is reaching the amorphous limit [3, 4]. Unfortunately, improvements to the power factor from the sharp features of the low dimensional density of states as suggested in Ref. [5] were not observed because small feature sizes enhance electron scattering and significantly reduce the electrical conductivity [6]. It was theoretically shown, however, that in NWs modulated by interconnected dots [7, 8, 9], or nanocomposite materials [10], an improvement in the power factor could be achieved. In those cases, the Seebeck coefficient increases in certain regions of the channel where filtering is more effective. Such effects can also exist in polycrystalline NW structures, which might offer an alternative approach in achieving simultaneous thermal conductivity reduction and power factor improvements through improvements in the Seebeck coefficient. In polycrystalline silicon an unexpected increase of the power factor with respect to single crystals was reported by some of our co-authors, which was related to the precipitation of a second phase around grain boundaries [11, 12]. Films of polycrystalline silicon deposited onto oxidized Si substrates were implanted with boron to a total nominal density of 4.4×10^{20} cm^{-3}. Samples were submitted to a sequence of annealing cycles in Ar, carried out at temperatures from 500 to 1000 °C in 100 °C steps, each treatment lasting two hours. After each annealing step, the electrical resistivity, Hall coefficient and thermopower were measured. A quite unexpected concurrent increase of the thermopower and conductivity was reported for heat treatments at temperatures above 800 °C. Upon annealing at 1000 °C a power factor of 15 mW $K^{-2}m^{-1}$ (a value more than three times higher than in Si nanowires) was measured.

In this paper, we report on a theoretical analysis of the thermoelectric performance of polycrystalline Si bulk and NW materials by considering both electron and phonon transport. Our goal is to provide explanations about these experimental measurements and identify

performance optimization directions. The simulations are calibrated with experiments for bulk and polycrystalline Si. Where needed, we have extracted parameters from atomistic simulations, and used them in macroscopic transport models. We have performed an analysis involving all relevant geometrical and structural features such as grain and grain boundary sizes, density, and barrier heights. We find that the reduction of feature sizes such as the grain size and the NW diameter results in strong reduction in the thermal conductivity. Interestingly, for optimized designs, the Seebeck coefficient can be improved significantly with the introduction of the grain boundaries of the polycrystalline geometry, while the electrical conductivity is only weakly affected. Consequently, the power factor increases. In such a way, *ZT* values even higher that the ones reported for monocrystalline Si NWs can be achieved.

The paper structure is as follows: In section II we describe the theoretical model. In section III, the results of the calculations are presented and they are compared with our experimental data for polycrystalline Si. Finally, we summarize our work and give the main conclusions in section IV.

II. THEORETICAL MODEL

(i) Electronic part:

The electrical conductivity and Seebeck coefficient within the linearized Boltzmann theory are given by the following expressions:

$$\sigma = q_0{}^2 \int_{E_0}^{\infty} dE \left(-\frac{\partial f_0}{\partial E} \right) \Xi(E), \tag{1a}$$

$$S = \frac{q_0 k_B}{\sigma} \int_{E_0}^{\infty} dE \left(-\frac{\partial f_0}{\partial E} \right) \Xi(E) \left(\frac{E - E_F}{k_B T} \right), \tag{1b}$$

where the transport distribution function $\Xi(E)$ is defined as [6, 13]:

$$\begin{aligned} \Xi(\varepsilon) &= N(\varepsilon) v(\varepsilon)^2 \tau(\varepsilon) \\ &= N(\varepsilon) v(\varepsilon) \left[v(\varepsilon) \tau(\varepsilon) \right] \\ &= N(\varepsilon) v(\varepsilon) \lambda_0 \left(E / k_B T \right)^r \end{aligned} \tag{2}$$

In Eq. (2) $v(E) = \partial E / \hbar \partial k_x$ is the bandstructure velocity, $N(E)$ is the 3D density of states, and $\tau(E)$ is the momentum relaxation time for a state at energy *E*. Here we employ the 3D

bandstructure and transport models derived for 3D carriers since our NWs are thick enough to resemble bulk (>10nm). As we indicated in a previous study, 1D features begin to appear in the electronic properties of Si NWs at diameters below 7nm [14].

In Eq. (2) the energy dependence of the mean-free-path (MFP) for scattering is introduced with a characteristic exponent *r* that defines the specific scattering mechanism:
(a) In the case of phonon scattering in 3D channels that is assumed here, the MFP is energy independent [15, 16], *r*=0 and consequently the scattering rate is just proportional to the density of states. Our simulation reproduces the p-type bulk Si low-field mobility $\mu_p = 450$ cm^2/V-s for $\lambda_0^{ph} = 7.4nm$ that is consistent with the MFP of holes in Si. (b) For impurity scattering we use the Brooks-Herring model as described in Ref. [16], the momentum relaxation rate is given by:

$$\tau(E) = \frac{16\pi\varepsilon_{Si}^2\sqrt{2m_{DOS}}}{q_0^4 N_I}\left(\ln\left(1+\gamma^2\right) - \frac{\gamma^2}{1+\gamma^2}\right)^{-1}\left(E-E_0\right)^{3/2} \qquad (3a)$$

where

$$\gamma^2 = \frac{8m_{DOS}\left(E-E_0\right)L_D{}^2}{\hbar^2} \qquad (3b)$$

and

$$L_D{}^2 = \frac{\varepsilon_{Si}^2 k_B T}{q_0^2 n}\frac{\Im_{1/2}\left(\eta_F\right)}{\Im_{-1/2}\left(\eta_F\right)} \qquad (3c)$$

In the expressions above, L_D is the screening length for 3D bulk ionized impurities, valid in both the non-degenerate, and degenerate limits as described in Ref. [17], N_I is the dopant (ionized impurity) concentration, $\Im_d\left(\eta_F\right)$ is the Fermi-Dirac integral of order *d*, and η_F is the reduced Fermi level $\left(E-E_0\right)/k_BT$. As described in Ref. [18], this approach seems to work satisfactory for doping concentrations up to 10^{18}/cm^3. To account for the strong screening at larger carrier concentrations we use the strongly screened transition rate as defined in [16]:

$$\tau(E) = \frac{\hbar}{\pi N_I}\left(\frac{\varepsilon_{Si}}{q_0^2 L_D{}^2}\right)^2\frac{1}{N(E)} \qquad (3d)$$

We note that the mean-free path for impurity scattering and the screening length at carrier concentrations above 10^{19}/cm^3, is only a few nanometers. These characteristic length scales, are smaller that the diameters/grain sizes we consider, and therefore we expect that the accuracy of the approach will be of similar as to what it is for bulk systems. Using the phonon and ionized impurity scattering as described above, the calculated mobility is in agreement with the experimental data for p-type Si bulk mobility [19, 20, 21]. In the case of NWs we include surface roughness scattering (SRS) using a simplified model, in which we define a

MFP λ_{SRS}^{0} for scattering of electrons near the interface of the NW. In narrow channels without fields, SRS originates from the shift of the band edges with confinement. Our atomistic simulations indicate that for a NW with a diameter *D*=3nm, this number is small $\lambda_{SRS}^{0} \sim 2\text{nm}$, but the effect of SRS is strongly reduced compared to phonon and impurity scattering as the diameter is increased above 10nm, and SRS is not anymore the dominant scattering mechanism. Nevertheless, we include the SRS MFP for completeness by assuming $\lambda_{SRS}^{ave}\left(E/k_BT\right)$ (although we mostly deal with grain sizes larger than 10nm). In our simplified model we assume that electrons residing spatially farther away from the surface of the NW and closer to the center, scatter with a larger SRS limited MFP, such that the average MFP for all electrons in the NW linearly increases with the radius of the NW.

The overall MFP is computed using Matthiessen's rule as:

$$\left[v(E)\tau(E)\right] = 1/\left[1/\left(\lambda_{ph}\left(E/k_BT\right)^{0}\right) + 1/\left(\lambda_{SRS}\left(E/k_BT\right)\right) + 1/\left(v(E)\tau_{imp}(E)\right)\right] \qquad (4)$$

(ii) Phonon thermal conductivity part:

We employ macroscopic treatment of phonons for the calculation of the phonon structure. The phonon transport is treated semiclassically within the Boltzmann transport equation. The thermal conductivity is calculated by summing contributions from all the wavevectors that belong to the first Brillouin zone and all phonon polarizations [22]. The relaxation time depends on the energy of the vibration mode, the temperature, and the system size. The total relaxation time is obtained by considering independent contributions from all scattering mechanisms. The relevant scattering mechanisms that have been included here are: i) Umklapp processes (phonon-phonon interactions), ii) phonon-defect interactions, and iii) scattering on the system boundaries. We employ parameters from the literature that fit the temperature dependence of the bulk Si thermal conductivity [22].

The boundary scattering is treated beyond the commonly used phenomenological model in the Casimir limit. The relaxation time due to boundary scattering is calculated for each wave vector by the phonon group velocity and the distance *L* that a phonon can travel between two boundary surfaces. It also depends on the surface roughness through a parameter *f* that accounts for the nature of the boundary (specular or diffuse). The distance *L* is determined for each phonon wave vector $\vec{k}$ by geometrically averaging over the wire cross section. The dependence of the parameter *f* on the specularity *p* of the scattering is fully taken into account as *f* = (1+*p*)/(1-*p*). The specularity parameter *p* depends on the wave vector *k* and

the boundary roughness η as $p = e^{-4k^2n^2}$. It varies from 1 (for specular boundary scattering) to 0 (for completely diffusive boundary scattering).

(iii) Polycrystalline material

Our theoretical model for polycrystalline material assumes a sequence of grains separated by grain boundary barriers. This resembles a 1D channel, or a NW, however the main findings will provide qualitative insight into the operation of bulk polycrystalline as well. In the case of the polycrystalline material, the transport happens through two phases, the crystalline grain and the grain boundary region, which is closer to an amorphous material. The total resistivity of the channel is the weighted average of the resistivities of the grain and grain boundaries, with the length of each region as the weighting factor. This model is common practice for polycrystalline materials and nanocomposites [23, 24]. In this work, we assume that it is still valid for the nanocrystalline structures that we consider as well. The electrical conductivity of the composite material is given by:

$$\frac{L_{tot}}{\sigma_{tot}} = \frac{L_G}{\sigma_G} + \frac{L_{GB}}{\sigma_{GB}}, \qquad (5)$$

where L_{tot}, L_G, L_{GB} and are the lengths of the entire structure, the grain and the grain boundary regions respectively, as indicated in Fig. 1a. The electrical conductivity in the grain boundary region is given by:

$$\sigma_{GB}(E) = 0 \qquad \text{for} \quad E <= V_b \qquad (6a)$$

$$\sigma_{GB}(E) = \sigma^0_{GB}(E) \qquad \text{for} \quad E > V_b \qquad (6b)$$

The model assumes that there is a barrier built on the amorphous grain boundary region, and transport is thermionic over that barrier. Any effects occurring at the interface could be lamped into the value of σ^0_{GB}, and effectively included as an additional series resistance. In this work however, we assumed that $\sigma^0_{GB}(E) = \sigma^0_G(E)$.

The Seebeck coefficient is determined by the combined transport in the grains and in the grain boundaries of the polycrystalline material. There are two regimes of transport: i) when electrons flow ballistically (without relaxing their energy) in the grain until they reach the grain boundary, and ii) When electron transport in the grains is diffusive (energy relaxation of carriers prevails). In the first case, the overall Seebeck coefficient is determined by the Seebeck coefficient of the highest barrier for carriers, which is the barrier introduced by the grain boundaries.

$$S_{E:not-relaxed} = S_{GB} \tag{7a}$$

In the second case, the Seebeck coefficient is determined by the weighted average of the Seebeck coefficients of the two regions, with the weighting factor being the temperature drop in each region, which we assume that it is determined by the thermal conductivity of the regions [10, 25, 26]:

$$S_{E:relaxed} = \frac{S_G T_G + S_{GB} T_{GB}}{T_G + T_{GB}} = \frac{S_G L_G / \kappa_G + S_{GB} L_{GB} / \kappa_{GB}}{L_G / \kappa_G + L_{GB} / \kappa_{GB}} \tag{7b}$$

In the case where transport is neither fully ballistic, nor fully diffusive, we follow a simple treatment and compute the overall Seebeck coefficient by weighting the two quantities, with the weighting factor being the percentage of energy relaxation in the grain, determined by the MFP of the energy relaxing processes, in our case the optical phonons [10, 27]. This is defined by [27]:

$$C = \frac{\lambda_E}{\lambda_E + L_G} \tag{8}$$

where λ_E is the MFP of the energy relaxing mechanisms, and L_G is the length of the grain region. For p-type Si, the value of C versus the length of the channel is shown in Fig. 1b. For channels around 30-50nm which are close to the grain sizes of our experimental data, the energy of the carriers is ~50% relaxed. The overall Seebeck coefficient is then given by:

$$S_{tot} = C S_{E:non-relaxed} + (1-C) S_{E:relaxed} \tag{9}$$

Finally, the ZT figure of merit is computed by:

$$ZT = \frac{\sigma S^2 T}{\kappa_e + \kappa_l} \tag{10}$$

III. RESULTS AND DISCUSSION

In polycrystalline Si, the grain boundaries drastically affect the dopant distribution, the electron, and the phonon transport. Energy barriers are built up at grain boundaries due to the crystal and structural inhomogeneities such as dopant segregation, imperfections etc. Energy selectivity could be provided by these energy barriers and lead to enhanced thermoelectric performance. The presence of energy barriers could interpret the experimental evidence on enhanced Seebeck coefficient and power factor. Moreover, thermal conductivity reduction and non-uniformity further contribute to the enhancement of ZT. A proper design of polycrystalline boundaries could prove beneficial for the power factor and ZT. Geometrical features such as the grain density, grain size, grain boundary size and density, as well as

electronic features such as the grain boundary height, or the grain boundary thermal conductivity compared to the thermal conductivity of the grain, could act as design parameters (see Fig. 1 for grain/grain-boundary model).

We first examine the effect of the grain boundary height on the thermoelectric coefficients. This is described in Fig. 2. As indicated in Fig. 2a, by increasing the barrier height from zero to V_b=0.2V and then to V_b=0.4V, a decrease in the conductivity from the bulk values (dotted line) is observed. The conductivity remains at low values for larger carrier concentrations when the barrier heights are increased, until the Fermi level in the channel is high enough for the carriers to be thermionically injected over the barrier. Once this happens, the conductivity sharply increases. The inset of Fig. 2a shows the low-field mobility of these channels. In the polycrystalline nanocomposite structures, the mobility drops significantly from the bulk values for low carrier concentrations since these carriers do not have enough energy to overpass the barrier heights. At high carrier concentrations, however, the carriers have enough energy to pass over the barriers, and the mobility values are mostly restored. On the other hand, an increase in the Seebeck coefficient is observed as shown in Fig. 2b. The barrier heights increase the ability of the material to filter carriers. Since the decrease in the conductivity mostly appears for low carrier concentrations, the power factor overall increases for higher concentrations (blue, red lines) compared to bulk (black dotted line) as observed in Fig. 2c. The peak in the power factor $S^2\sigma$, is however, narrower, and also shifts to high carrier concentrations. The change in the *ZT* due to the introduction of the barriers alone, is shown in Fig. 2d. The *ZT* increases to ~0.06, compared to the bulk value of <0.01. This increase is solely due to the existence of energy barriers for the electron transport. The bulk phonon thermal conductivity κ_l=140W/mK is still assumed. As it will be shown below, large improvements in the *ZT* could be obtained when the reduction of κ_l due to the grain effects is also taken into account.

From Eq. (7b), it is expected that the Seebeck coefficient can be altered independently of the electrical conductivity once the thermal conductivity changes differently in the grains and in the grain boundaries. Since the overall Seebeck coefficient is weighted over the temperature drop in the different regions, the Seebeck coefficient in the regions with low thermal conductivity is important. Therefore, by allowing a drastically smaller thermal conductivity in the grain boundaries (where the Seebeck coefficient is larger) compared to the grains, the overall Seebeck coefficient can be increased, which increases the power factor in all carrier concentration ranges as well [10, 25]. This is shown in Fig. 3. Figure 3a shows the electrical conductivity for a channel with grains of L_G=50nm and V_b=0.2eV. Figure 3b shows

the Seebeck coefficient for two cases: i) The thermal conductivity in the grains and the grain boundaries is the same and equal to the bulk value κ_l =140W/mK (solid lines). ii) The thermal conductivity in the grains is kept at the bulk value κ_G=140W/mK, whereas that in the grain boundaries is reduced by a factor of 10 at κ_{GB}=14W/mK (black-dotted line). The Seebeck coefficient increases once the two thermal conductivities differ. The electrical conductivity, however, is independent of κ_l at first order, and is not affected. The power factor in Fig. 3c therefore increases (dotted-line) compared to the case where the thermal conductivities are the same (solid line). This significantly increases the *ZT* figure of merit by a factor of ~3 as indicated in Fig. 3d.

As of now, we have described how the variations in the barrier height and the thermal conductivity introduced by the grain boundaries can provide increases in the Seebeck coefficient without significantly reducing the electrical conductivity (at large carrier concentrations). This can increase the thermoelectric power factor and the *ZT* figure of merit. For illustration purposes, we have used arbitrary values for the barrier heights and the thermal conductivity. In what follows, we provide calculations in which the lattice thermal conductivities in the grains and in the grain boundaries have been calculated for the actual grain geometry using the approach described in Section II. Grains of different sizes will exhibit different thermal conductivities. We consider four grain size cases and computed the following thermal conductivities: i) L_G=100nm, κ_G=20 W/mK, κ_{GB}=9W/mK, ii) L_G=50nm, κ_G=12W/mK, κ_{GB}=6W/mK, iii) L_G=30nm, κ_G=8W/mK, κ_{GB}=4.5W/mK, iv) L_G=10nm, κ_G=2.7W/mK, κ_{GB}=1.7W/mK. The thermal conductivity decreases drastically with decreasing grain size due to the modification of the phonon bandstructure, which results in a smaller number of contributing phonons, and the increased phonon boundary scattering. In addition, in the grain boundaries, phonons are scattered more strongly by the high concentration of dopants, dislocations, and imperfections.

Figure 4 shows the thermoelectric coefficients for the geometries with grain and grain boundary sizes as described above. In this case we keep the grain boundary height fixed at V_b=0.2V. Figure 4a shows the electrical conductivity versus carrier concentration. The conductivity of p-type bulk Si is indicated by the dotted line. When the grains are introduced into the channel, the conductivity degrades for the lower carrier concentrations, but this degradation is reduced as the carrier concentration is increased. In the case of the smallest grains, the conductivity can even increase above the bulk level because in that case due to the high density of grain boundary barriers, the Fermi level is pushed deep into the bands for the same carrier concentration. The carriers contributing to transport have then higher energies

and the electrical conductivity increases. Figure 4b shows the Seebeck coefficient, which increases as the grain sizes decrease. The increase in the Seebeck coefficient with reduction in the grain size compared to bulk (dotted line) is a result of both, the increase in the grain boundary density, and the increase in the thermal conductivity ratio between the two regions. The power factor is shown in Fig. 4c. Due to the large increase in the Seebeck coefficient, a substantial power factor increase is achieved as the grain sizes become smaller. Large values in the *ZT* can also be achieved as shown in Fig. 4d. For grain sizes of 30nm, the *ZT* can reach 0.5. However, for smaller grains, where the thermal conductivity can be reduced to κ_l=2.7W/mK, the *ZT* can reach values as high as 2.5. We mention that such low values in thermal conductivity were achieved for monocrystalline Si nanowires [1, 2]. In that case, *ZT* values of 0.5 were achieved. Here, in the case of polycrystalline nanowires, the increased carrier filtering capabilities of this structure, and the additional influence of the lower thermal conductivity of the grain boundaries on the Seebeck coefficient, together with the overall drastic reduction in the thermal conductivity, can provide even higher *ZT* values.

In Fig. 4, our experimental measurements for the electrical conductivity and the Seebeck coefficient for structures with average grain size 30nm are shown by the blue dots. The measurements were performed at room temperature, but each dot presents structures that were processed under different annealing temperatures. With increasing annealing temperature, the carrier concentration decreases, the conductivity increases slightly with concurrent significant increases in the Seebeck coefficient and in the power factor. The experimental dependence of the conductivity and of the Seebeck coefficient was previously attributed to the modification of the energy dependence of the mobility in the polycrystalline material [28]. The increase of the Seebeck coefficient can be, however, better accommodated within the present theoretical model. As the annealing temperature increases, the dopants move towards the grain boundaries and the barrier heights are increased [23]. The high concentration of impurities in the barriers, and their close to amorphous nature, also increases the number of scatterers for phonons resulting in decreasing thermal conductivity in the grain boundary and increasing ratio of the thermal conductivity between the grain and the grain boundary. As shown in Fig. 2, when the barrier height increases the electrical conductivity does not change substantially at the larger carrier concentration regions, while the Seebeck coefficient and the power factor do increase more significantly. This effect together with the estimated non-uniform reduction in the thermal conductivity explain the measured increase in the Seebeck coefficient for average grain sizes of 30 nm, as it is shown in Fig. 4b. The exact values for the achieved Seebeck coefficient are a function of the exact barrier heights,

impurity and dopant concentrations, and grain and grain boundary sizes. A better quantitative explanation of the measured values will depend on these geometrical and electronic/thermal distributions, as well as by taking into account that the measured data is taken from a polycrystalline bulk material. Our simple model, however, that considers a uniform 1D chain of grains and grain boundaries reveals the basic underlying physical mechanisms and provides explanation of the large increase in the measured Seebeck coefficient and power factor in poly-Si.

Finally, we mention the assumptions we have used in our model: i) Semiclassical treatment of transport where transport is thermionic over the barriers, ii) Bulk Si bandstructure, that is retained even under high doping concentrations, iii) Simplified rectangular treatment of the grain boundary energy barrier, iv) Flat energy profile in the grain. v) Other than the effect of the barrier height, no additional reduction is considered for the electrical conductivity on the interfaces of the grain / grain-boundaries. These simplifications are commonly used in assessing the transport properties of polycrystalline materials and to interpret experimental data. Although a more sophisticated model could provide quantitatively more reliable estimations, we do not expect our main conclusions to be affected. We note that our intention is to provide qualitative insight into the effects that could provide power factor improvements in nanocrystalline poly-Si NWs, and not necessarily numbers. We believe that our simple model reveals these basic underlying physical mechanisms and could provide design guidance for performance enhancement.

IV. SUMMARY AND MAIN CONCLUSIONS

We have investigated theoretically electron and phonon transport in polycrystalline Si with grain sizes below 100nm in order to interpret experimental measurements. Our theoretical model for polycrystalline NWs assumes a sequence of grains separated by grain boundary barriers. We have performed an analysis involving relevant geometrical and structural features such as grain and grain boundary sizes, barrier heights, and impurity concentration. We show that the measured enhancement of the Seebeck coefficient and power factor can be interpreted in terms of the built-up grain boundary barriers and the non-uniform decrease in the thermal conductivity in the grains and in the grain boundaries (i.e. larger decrease in the thermal conductivity of the grain boundaries). A drastically smaller thermal conductivity in the grain boundaries (where the Seebeck coefficient is larger) compared to the grains leads to an increase in the macroscopic Seebeck coefficient – and to an increase of the

power factor in all carrier concentration ranges. Our findings suggest that the Seebeck coefficient and consequently the power factor can be improved significantly once the polycrystalline geometry is properly optimized, while avoiding strong reduction in the electrical conductivity. In such a way, even larger *ZT* improvements can be achieved in polycrystalline Si NWs compared to monocrystalline NWs.

ACKNOWLEDGMENT

The authors acknowledge the financial support by the Consorzio DeltaTi Research.

REFERENCES

[1] A.I. Boukai, Y. Bunimovich, J. T.-Kheli, J.-K. Yu, W. A. G. III, and J. R. Heath, Nature, 451, pp. 168-171, 2008.

[2] A. I. Hochbaum, R. Chen, R. D. Delgado, W. Liang, E. C. Garnett, M. Najarian, A. Majumdar, and P. Yang, Nature, 451, pp. 163-168, 2008.

[3] C. J. Vineis, A. Shakouri, A. Majumdar, and M. C. Kanatzidis, Adv. Mater., 22, 3970-3980, 2010.

[4] K. Nielsch, J. Bachmann, J. Kimling, and H. Boettner, Adv. Energy Mater., 1, 713-731, 2011.

[5] L.D. Hicks, and M. S. Dresselhaus, Phys. Rev. B, 47, no. 24, p. 16631, 1993.

[6] N. Neophytou and H. Kosina, Phys. Rev. B, 83, 245305, 2011.

[7] X. Zianni, Appl. Phys. Lett., 97, 233106, 2010.

[8] X.Zianni, AIP Conf. Proc., 1449, 21 (2012); doi: 10.1063/1.4731487.

[9] X. Zianni, J. Solid State Chem., 193, 53, 2012.

[10] R. Kim and M. Lundstrom, J. Appl. Phys. 110, 034511, 2011.

[11] D. Narducci, E. Selezneva, G. Cerofolini, E. Romano, R. Tonini, and G. Ottaviani, MRS Symp. Proc., 2010, 1314, mrsf10-1314-ll05-16.

[12] D. Narducci, E. Selezneva, G. Cerofolini, S. Frabboni, and G. Ottaviani, J. Solid State Chem., 193, 19, 2012.

[13] T. J. Scheidemantel, C. A. Draxl, T. Thonhauser, J. V. Badding, and J. O. Sofo, Phys. Rev. B, 68, p. 125210, 2003.

[14] N. Neophytou and H. Kosina, Phys. Rev. B, 84, 085313, 2011.

[15] R. Kim, S. Datta, and M. S. Lundstrom, J. Appl. Phys., 105, p. 034506, 2009.

[16] M. Lundstrom, "Fundamentals of Carrier Transport," Cambridge University Press, New York, 2000.

[17] H. Kosina and G. K.-Grujin, Solid State Electron., 42, 3, 331-338, 1998.

[18] A. T. Ramu, L. E. Cassels, N. H. Hackman, H. Lu, J. M. O. Zide, and J. E. Bowels, J. Appl. Phys., 107, 083707, 2010.

[19] C. Jacoboni and L. Reggiani, Rev. Mod. Phys., 55, 645, 1983.

[20] http://www.ioffe.ru/SVA/, "Physical Properties of Semiconductors".

[21] G. Masetti, M. Severi, and S. Solmi, IEEE Trans. Electr. Dev., 30, 764, 1983.

[22] P.Chantrenne, J.L.Barrat, X.Blase, J.D.Gale, J.Appl. Phys., 97, 104318, 2005.

[23] J. W. Orton and M. J. Powell, Rep. Prog. Phys. 43, 1263, 1980.

[24] F. V. Farmakis, J. Brini, G. Kamarinos, C. T. Angelis, C. A. Dimitriadis, and M. Miyasaka, IEEE Trans. Electr. Dev., 48, 701, 2001.

[25] M. Zebarjadi, G. Joshi, G. Zhu, B. Yu, A. Minnich, Y. Lan, X. Wang, M. Dresselhaus, Z. Ren, and G. Chen, Nano Lett., 11, 6, pp 2225–2230, 2011.

[26] J. Jerhot and J. Vlcek, Thin Solid Films, 92, 259, 1982.

[27] M. Lundstrom, Electr. Dev. Lett., 22, 6, 293-295, 2001.

[28] D. Narducci, E. Selezneva, G. Cerofolini, E. Romano, R. Tonini, and G. Ottaviani, Proceedings of the 8th European Conference on Thermoelectrics (ECT2010), p.141-146, 2010.

Figure 1

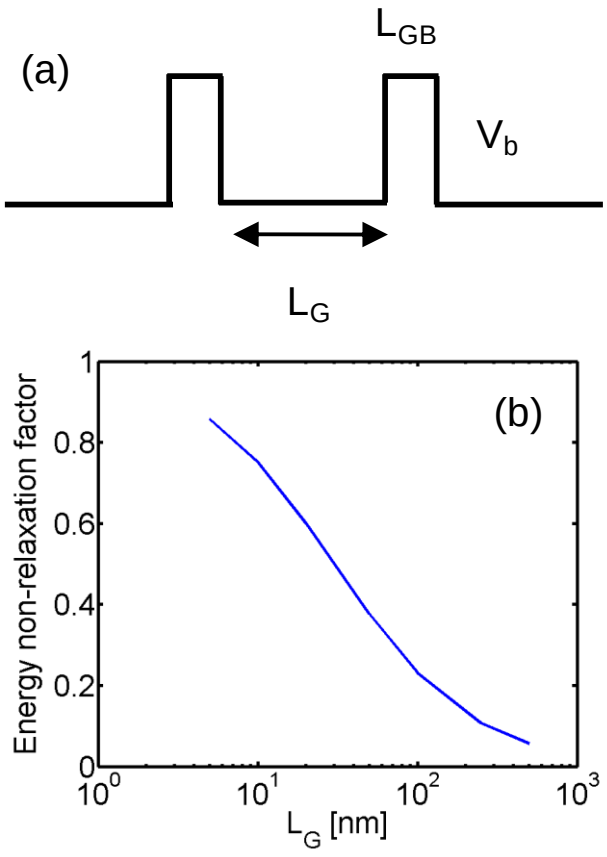

Figure 1 caption:

(a) The nanocomposite polycrystalline model, consisting of grain and grain boundaries. L_G is the length of the grain region and L_{GB} the length of the grain boundary region. (b) The factor that specifies how much of the carrier energy relaxes in the grain as a function of the grain length.

Figure 2:

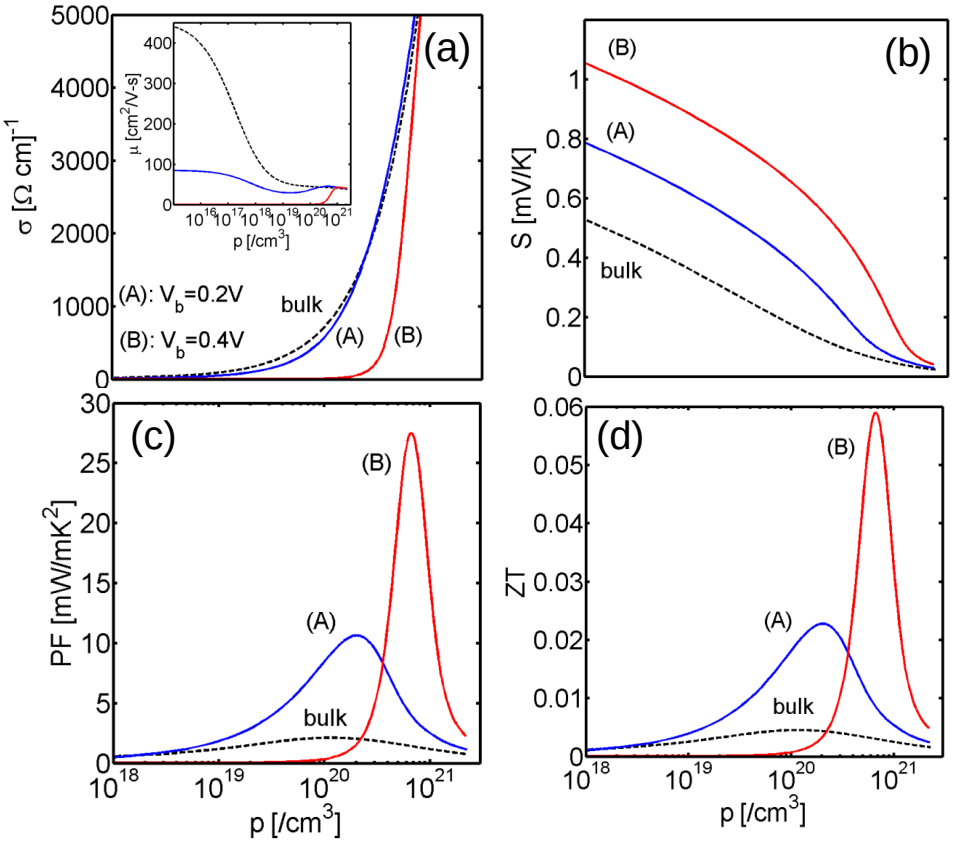

Figure 2 caption:

The effect of the grain boundary size on the thermoelectric coefficients of the polycrystalline nanocomposite structure with L_G=50nm and L_{GB}=3nm. Black dotted lines: Monocrystalline p-type bulk Si. Blue line, labelled (A): V_b=0.2V. Red line, labelled (B): V_b=0.4V. (a) The electrical conductivity versus carrier concentration. (b) The Seebeck coefficient. (c) The power factor. (d) The *ZT* figure of merit. Inset of (a): The mobility of each structure versus carrier concentration.

Figure 3:

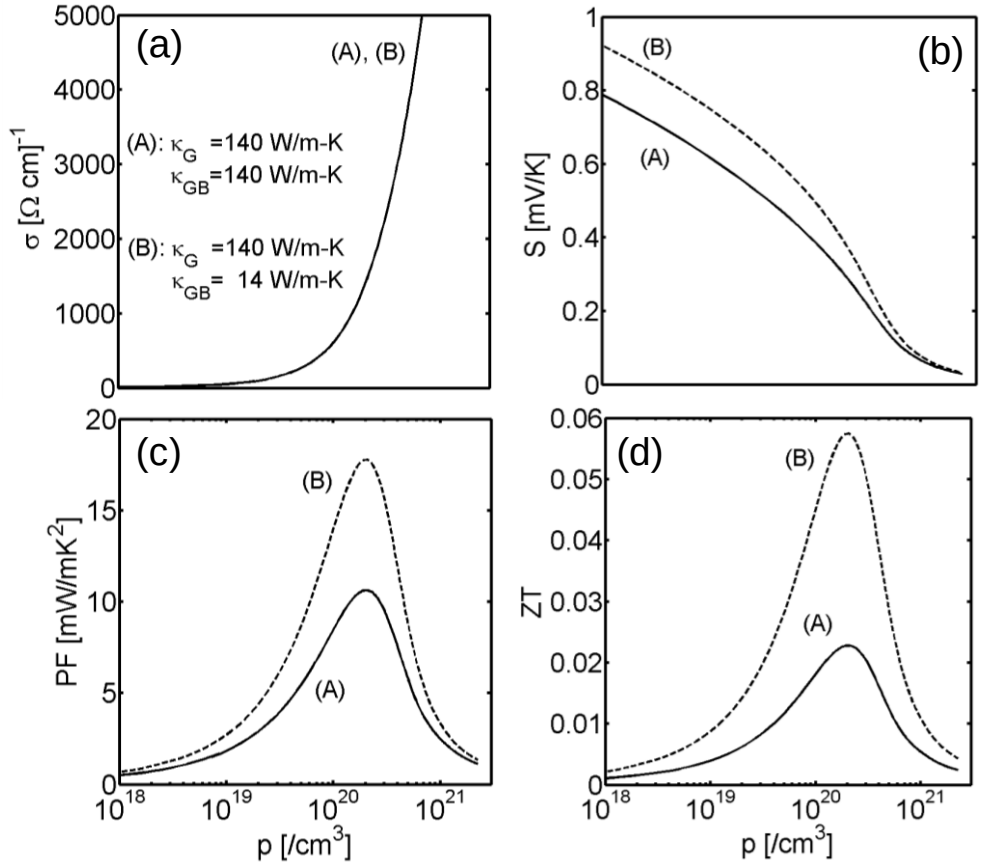

Figure 3 caption:

The effect of the lower thermal conductivity in the grain boundary compared to the thermal conductivity in the grain on the thermoelectric coefficients of the polycrystalline nanocomposite structure with L_G=50nm, L_{GB}=3nm, and V_b=0.2eV. Black solid lines labelled (A): $\kappa_{GB}=\kappa_G$=140W/mK. Dashed line, labelled (B): $\kappa_{GB}=\kappa_G/10$=14W/mK. (a) The electrical conductivity versus carrier concentration. (b) The Seebeck coefficient. (c) The power factor. (d) The *ZT* figure of merit.

Figure 4:

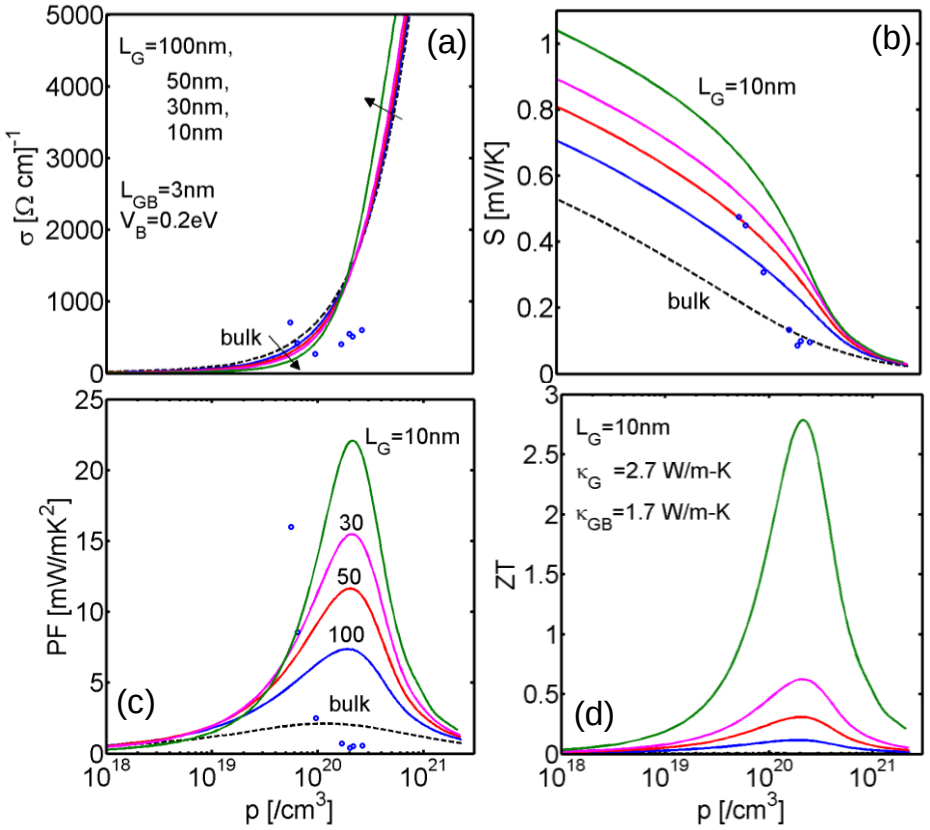

Figure 4 caption:

Thermoelectric coefficients for structures of different grain sizes, with their corresponding calculated thermal conductivity, as well as the corresponding thermal conductivity of the grain boundaries. Grain sizes of L_G=100nm (blue), L_G=50nm (red), L_G=30nm (magenda), and L_G=10nm (green) are shown (from top to bottom in b, c, d). Dashed lines represent the p-type bulk Si results. (a) The electrical conductivity versus carrier concentration. (b) The Seebeck coefficient. (c) The power factor. (d) The *ZT* figure of merit. Blue dots: Experimental data for a material close to the L_G=30nm case measured at room temperature, but under different annealing conditions.